

J. O. Peralta

División de Posgrado
Facultad de Ingeniería
Universidad del Zulia
Venezuela.

Radial-Velocity Dispersion as a Function of Galactic Longitude and Distance

(Recibido el 10 de Enero, 1978)

RESUMEN

Dispersiones de velocidad radial de diferentes muestras de estrellas de la Población I se comparan con la cantidad teórica $\Delta V = V_{\max} - V_{\min}$ obtenida a partir de las áreas permitidas en los diagramas de velocidad radial versus longitud galáctica. Se ve que el valor observado ΔV es aproximadamente tres veces la dispersión de velocidad definida por

$$\sigma_v = \left[\sum_i (v_i - \bar{v})^2 / n \right]^{1/2}$$

En el caso de las supergigantes, las desviaciones con respecto a la dispersión teórica sugieren la posibilidad de errores en la determinación de distancias para ciertas longitudes galácticas. Se analizan también los valores medios y las dispersiones de los residuos. Existe una buena correlación entre la dispersión de los residuos y la cantidad teórica $\Delta V / 2$ en el diagrama velocidad versus longitud. Se observa que las direcciones, en las que se presentan grandes desviaciones respecto del comportamiento teórico predicho, coinciden con algunos picos de la curva que representa la distancia del objeto más lejano como función de la longitud. Ningún intento se hace por interpretar los resultados dentro del contexto de la teoría de ondas de densidad de Lin.

SUMMARY

Radial-velocity dispersions of different samples of Population I stars are compared to the theoretical quantity $\Delta V = V_{\max} - V_{\min}$

derived from the permitted areas in the radial velocity versus galactic longitude diagrams. It is seen that the observed ΔV is roughly three times the observed velocity dispersion as defined by

$$\sigma_v = \left[\sum_i (v_i - \bar{v})^2 / n \right]^{1/2}$$

Departures from the theoretical dispersion in the case of supergiants suggest the possibility of errors in the determinations of distances at some galactic longitudes. Mean values and dispersions of residuals are also analyzed. There is a good correlation between the dispersion of the residuals and the theoretical quantity $\Delta V / 2$ in the velocity versus longitude diagram. It is observed that the directions in which large departures from the predicted kinematical behaviour occur coincide with some of the peaks of the curve that represents the distance of the farthest object plotted against longitude. No attempt is made to interpret the results in the context of Lin's density-wave theory.

Key words: Radial velocity, star distances, non-circular motions, galactic kinematics.

1. INTRODUCTION

We shall discuss in this paper the velocity dispersion of different samples of stars in the framework of the theory of permitted areas of radial velocities.

The extension of the concept of permitted areas to non-circular orbits (Peralta, 1977a, b) enables us to predict the radial-velocity dispersion as a function of galactic longitude and distance. For a given direction ℓ in the galactic plane, the width of the permitted area depends on the maximum distance observed in that direction, the maximum orbital eccentricity of the sample of stars, and the galactic longitude ℓ . If the distances of the stars of the sample are accurately known, the maximum orbital eccentricity may be easily determined. It is evident that a sample of neighbouring stars is more suitable for determining the maximum eccentricity since short heliocentric distances are more reliable than large ones. If we now assume that the maximum orbital eccentricity is nearly the same at all distances we can compare the observed dispersion, measured as the width of the permitted area or as the quantity σ_v previously defined, and the theoretical value

$$\Delta V = V_{\max} - V_{\min}.$$

In the present discussion streaming motions as predicted by the density-wave theory are not taken into account. This is equivalent to assuming that the velocity amplitudes of the wave, if it exists, are small enough to be hidden by the observational errors and the averaging methods for analyzing the optical data. Since the amplitude of the density wave can only be determined by observation, the velocity amplitudes of the radial and tangential components of the perturbation remain uncertain up to the present. Thus, under reasonable assumptions, predicted values for the velocity amplitudes of less than 1 km/s in the case of stars cannot be considered as unrealistic (Wielen, 1974).

The optical data for this investigation were taken from Humphreys' (1970) catalogue, the set of 512 FK4/FK4 Sup stars studied by Fricke *et al.* (1975), and the sample of cepheids from Geyer's (1970) catalogue. Only stars with $|b| \leq 10^\circ$ are considered.

2. VELOCITY DISPERSION AND PERMITTED AREAS.

Let us consider the difference $\Delta V = V_{\max} - V_{\min}$ between the extreme values of radial velocities, which define the permitted area, for a given heliocentric distance r , galactic longitude ℓ , and maximum orbital eccentricity e . Assuming that all the stars of a given sample are at nearly the same distance r from the sun, ΔV becomes a function of galactic longitude only. Figure 1 shows the run of ΔV

for different distances and eccentricities. When comparing Figs. 1a and 1b the response of ΔV to varying the gravitational potential becomes evident. Two types of gravitational potential are considered: that of Eggen *et al.* (1962) and the one derived from Contopoulos-Strömberg formula (1965). Their corresponding rotation curves are shown in Figure 2. The run of ΔV when plotted against ℓ is nearly independent of r when the galactic potential is that of Eggen *et al.*, while in the second case ΔV is quite sensitive to heliocentric distances in the longitude sector $80^\circ \lesssim \ell \lesssim 280^\circ$.

Let us now analyze the integrated radial-velocity dispersion when observing any given direction ($\ell, b = 0^\circ$) in the galactic plane. Since we are observing a superposition of permitted areas corresponding to different heliocentric distances, ΔV must be greater than that corresponding to any particular distance.

Figures 3 and 4 show the integrated ΔV plotted against galactic longitude; the heliocentric distance r and the maximum eccentricity e are taken as parameters. It is also shown in Figure 3, for comparison, the integrated ΔV when only circular orbits are assumed. In this case the variation of distance is the only source of dispersion in velocity.

Given a large sample of Population I stars, the contours of the observed permitted area in the diagram radial velocity versus longitude depend on the maximum distance observed at a given longitude: The larger the maximum distance the larger the width ΔV of the permitted area. If our sample had a roughly homogeneous distribution in distances in the range, say $0 < r \leq r_m$, the observed ΔV would be a smooth curve such as one of those shown in Figure 3 defined by the parameter r_m . In practice, ΔV is an irregular curve since the maximum observed distances of the sample's stars are not the same for all longitudes. We may compare the observed permitted area defined by the extreme values of the velocity observed and the theoretical one. In Figure 5a the velocity pattern of stars taken from the catalogues of Fricke *et al.* (1975) and Geyer (1970) is shown together with a tentative observed permitted area. The stars are located at distances in the range $0.3 \leq r \leq 0.7$ kpc. The comparison of the observed and theoretical ΔV is shown in Figure 5b. A similar analysis is done for stars in the distance interval 0 - 0.1 kpc. The comparison of the observed and theoretical ΔV is shown in Figure 5b. A similar analysis is done for stars in the distance interval 0 - 1 kpc in Figure 6. Figure 7 illustrates the case of 50 B- nebulae studied by Greig (1972) with calculated distances in the range $0 < r \leq 3.5$ kpc.

The observed ΔV of a sample of supergiants from Humphreys' (1970) catalogue are shown in Figures 8, 9, and 10. Three different situations are illustrated, namely; $r \leq 2$ kpc, $r \leq 3$ kpc, and $r \leq 5$ kpc. Theoretical curves are also shown for comparison for each case. We assume a maximum orbital eccentricity of 0.07 for this stellar group. An inspection of these figures reveals that the observed dispersion around $\ell = 115^\circ$ is higher than the predicted one, for $r \leq 2$ kpc and $r \leq 3$ kpc, while around $\ell = \pm 30^\circ$ the situation is the opposite. Systematic errors in the calculated distances may be the plausible explanation (the assumed members of the associations Cas OB2 and Per OB1 are responsible for this high dispersion around $\ell = 115^\circ$).

This method of analyzing the integrated permitted areas strongly depends on the extreme values of the observed radial velocities in the radial velocity/longitude diagram. A somewhat similar method is the comparison of ΔV -curves with the velocity dispersion σ_v which is expected to run in a similar way to ΔV . By definition, σ_v takes into account all the radial velocities in a given direction, ℓ . In order to compare σ_v with the observed ΔV in the case of supergiants, we use in Figures 11, 12, and 13, the quantity $3\sigma_v$. The σ_v -curves were found by taking 20° longitude sectors in such a way that two adjacent intervals are superimposed 10° . Because of the presence of observational errors a detailed correlation is not expected, but a good agreement in the large-scale trends of the observed and theoretical patterns is evident. At least up to a heliocentric distance of 3 kpc, σ_v is roughly of the order of one third of ΔV the width of the permitted area in a given direction.

In Figure 14 we have plotted the distance of the farthest star the sample against galactic longitude along with the σ_v -curves discussed in this paper. There are several narrow peaks in the velocity-dispersion curves which coincide in direction with those in the maximum-distance curve. These peaks may be interpreted as representing "windows" in the interstellar medium through which we can easily see large-distance objects.

3. KINEMATICAL TREND OF VELOCITY RESIDUALS.

The velocity residual defined as the difference $\Delta V_R = V_{obs} - V_{model}$ is generally used as an indicator of streaming motions in the stellar velocities. In an axisymmetrical gravitational potential, the individual departures of the observed velocities from the calculated ones are due to the following causes:

- stars are not describing perfect circular orbits,
- statistical errors in distance determinations and radial-velocity measurements,
- incorrect rotation model.

Let us assume for a while that we have error-free radial velocities and distances. In this situation the individual departures or "residuals" cannot be considered as genuine fluctuations in a statistical sense and they must represent the natural spread of orbital eccentricities. Consequently, residuals must be related to the kinematical trend of the permitted areas: statistically, their dispersion is expected to run in a similar way to $\Delta V/2$ when plotted against galactic longitude. In other words, the dispersion of residuals σ_R calculated in the similar way the quantity σ_v was obtained, must follow the run of ΔV in Figure 1a or 1b with an order of magnitude of about $\Delta V/2$. We shall discuss the average and the dispersion of residuals of 775 stars contained in the catalogues of Humphreys (1970), Fricke *et al.* (1975), and Geyer (1970). Again, 20° longitude sectors superimposed 10° are taken for calculating σ_R . We shall first analyze separately the group of supergiants since many of these stars have rather large spectrophotometric distances. Figures 15 and 16 show the trends of σ_R and $\overline{\Delta V}_R$ of these objects for different heliocentric distances. The values $U = -9$, $V = 16$ km/s have been adopted for the components of the solar motion. For comparison the trend of $\overline{\Delta V}_R$ for a different value of the V-component of the solar motion is also shown in Figure 16b. A plot of σ_R calculated by taking 10° longitude sectors superimposed 5° is illustrated in Figure 15. The response of σ_R to the chosen gravitational potential is shown in Figure 17 for two groups of supergiants. Except for very distant objects, the kinematical behaviour of σ_R does not substantially depend on the choice of one of the two potential discussed in this paper.

The behaviour of the average and dispersion of residuals for the rest of our whole sample of 775 stars with $|b| \leq 10^\circ$ is shown in Figure 18. In this case we have adopted for the components of the solar motion the values $U = -9$, $V = 12$ km/s (a somewhat larger value for the V-component may be adopted for these samples). Solar motion is a secondary matter in this discussion since it does not affect the dispersion of residuals as long as the longitude sectors, adopted for the calculations, are kept small.

In Fig. 19 our total sample of 775 stars, including all distances, is analyzed, while Fig. 20 shows the distance effect on σ_R and $\overline{\Delta V}_R$ by excluding the objects closer to the sun. We are now able to discuss the main features of the kinematical trend of the quantity defined as residual.

In accordance with Fig. 11 a value between 0.05 and 0.07 might be a reasonable estimate for the maximum orbital eccentricity of supergiants. There is a very good agreement in the orders of magnitude of σ_R and $\Delta V/2$ when an eccentricity of 0.05 is adopted. However, this

fact does not entitle us to conclude that 0.05 is the orbital eccentricity of our sample. The uncertainty in the value of e (which, otherwise, may be considered as a "natural" uncertainty, in the sense that there is not a sharp cut-off in eccentricities) prevents us from finding the constant of proportionality between σ_R and $\Delta V/2$. Nevertheless, the kinematical trend of the dispersion of residuals seems to behave in the way predicted by the theory of permitted areas of radial velocities.

Figures 21 and 22 summarize the present discussion on the statistical behaviour of the velocity residuals. For the sake of clarity, only theoretical curves for $e = 0.05$ are shown.

In Figure 22 σ_R becomes flatter than that corresponding to the sample of supergiants in Figure 21. Differences in the maximum orbital eccentricities of the samples of stars may be a plausible explanation.

The mean statistical fluctuations of $\overline{\Delta V_R}$ and σ_R for the group of 775 stars are, on the average, not greater than 5 km/s. But these fluctuations become considerably larger when only very distant objects are considered (see Figures 20a, b, and c). A careful examination of Figure 20c shows that the trends of σ_R and $\overline{\Delta V_R}$ of distant supergiants, modulate to some extent the kinematical response of the whole group of stars as is seen in Figures 15 and 16a.

The maximum predicted for $\Delta V/2$ at $\ell = 0^\circ$ is clearly observed in σ_R , but the minima at $\ell \cong 30^\circ$ and $\ell \cong 280^\circ$ are not evident for the sample of stars studied in this paper. However, for samples of closer objects these minima might become observable (see Figure 18). It is important to note that the two bulges in σ_R , around $\ell = 110^\circ$ and $\ell \cong 240^\circ$, which coincide with two "windows" or peaks in the maximum observed distance, might be hiding the two predicted minima.

It is important to point out here that the star distances are calculated values based on an assumption on the interstellar absorption, whereas the dispersion of residuals σ_R depends on these calculated values and

the observed radial velocities. Since theoretically, σ_R must be a smooth curve, the presence of peaks and bulges in the curve, coinciding with some of the "windows", tempts us to conclude that systematic errors in distance determinations, rather than in radial velocities, are present in those directions in which large-distance objects are observed (see Fig. 23).

The low values of σ_R , in the anticenter direction, compared with the maximum value at $\ell = 0^\circ$, seem to favour the gravitational potential derived from the Contopoulos-Strömberg formula, since, in the case of this potential and around the galactic anticenter ΔV decreases as heliocentric distance increases.

Finally, we shall briefly discuss the role given to the residuals as indicators of systematic motions. It is important to recognize that the only situation in which the average of residuals becomes zero is when the number of stars involved is very large and velocities and distances are accurately known. In this case, the velocity-points within the permitted areas must be homogeneously distributed. If the sample is not large enough, fluctuations and even "trends" may be present, indicating that the velocity-points are not evenly distributed around the circular velocity within the permitted areas. The behaviour of $\overline{\Delta V_R}$, shown in this paper, seems to indicate that the indiscriminate use of velocity residuals as indicators of systematic motions may be unsafe, since they could be representing a normal departure from circular motion, specially when studying a small number of stars or a small region in the galactic plane. If we intend to interpret kinematical trends with amplitudes lower than say, 7 km/s, as an indication of large-scale structures of our galaxy, we must keep in mind the presence of sources of velocity fluctuations with even larger amplitudes.

ACKNOWLEDGMENTS

Part of this work was carried out during a stay at the Astronomisches Rechen-Institut, Heidelberg. The author wishes to thank all members of the Institute for their hospitality. The calculations were carried out on IBM 370/145 at the Universidad del Zulia, Venezuela.

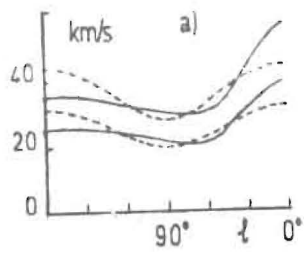


Fig. 1b

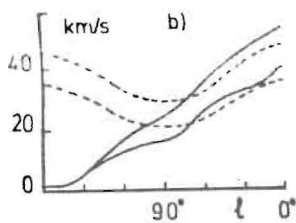


Fig. 1. The width of permitted areas plotted against galactic longitude for different heliocentric distances r and eccentricities e . a) The gravitational potential of Eggen *et al.* (1962) is assumed. The upper pair of curves at $\ell = 0^\circ$ corresponds to $e = 0.07$ and the lower pair to $e = 0.05$. Solid lines correspond to $r = 6$ kpc. Dashed lines correspond to $r = 0.1$ kpc. b) The same as in Figure 1a assuming a gravitational potential derived from Contopoulos-Strömberg formula (1965).

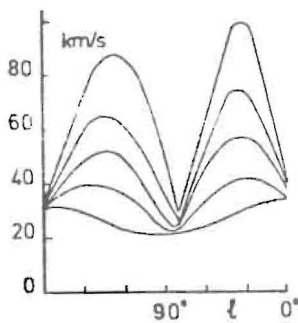


Fig. 4. The same as in Fig. 3 for $e = 0.05$ and heliocentric distances 5, 3, 2, 1, 0.1 kpc starting from above.

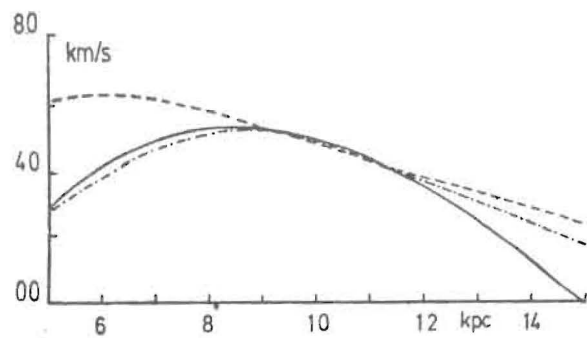


Fig. 2. Rotation curves of our Galaxy derived from the gravitational potential of Eggen *et al.* (dashed lines) and the Contopoulos-Strömberg formula (solid lines). Dotted-dashed line represents the Schmidt (1965) model.

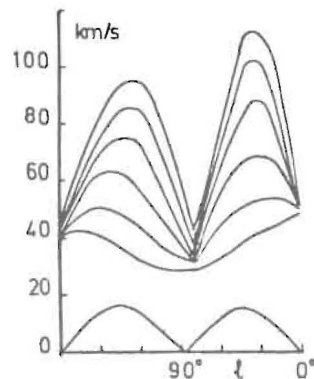


Fig. 3. The width of the permitted areas for a range of distances $0 - r$, obtained by superimposing all the permitted areas corresponding to all the distances within the interval $0 - r$ (integrated ΔV). The maximum orbital eccentricity assumed is 0.07. The corresponding distances r for the curves from above are: 5, 4, 3, 2, 1, 0.1 kpc. The lowermost curve represents the integrated ΔV for $r = 1$ kpc when only circular orbits are assumed. Since the curves are symmetric respect to $\ell = 0^\circ$, the longitude interval $180^\circ < \ell < 360^\circ$ has been omitted.

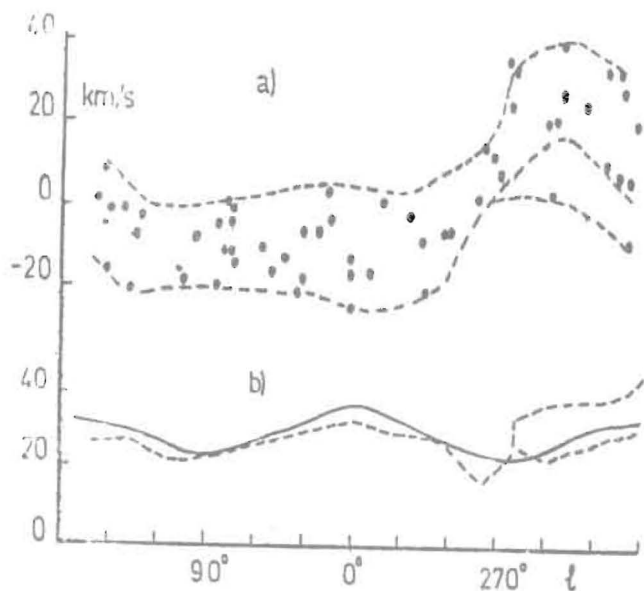


Fig. 5. a) Tentative observed permitted area of stars taken from catalogues of Fricke *et al.* (1975) and Geyer (1970). The stars are located within the distance interval 0.3 - 0.7 kpc. Two possible contours around $l = 200^\circ$ are drawn. b) As an approximation it is assumed that all the stars of Fig. 5a are located at $r = 0.5$ kpc. The theoretical width of the permitted area (solid line) for $e = 0.05$ and $r = 0.5$ kpc is compared with the observed width obtained from Fig. 5a (dashed lines).

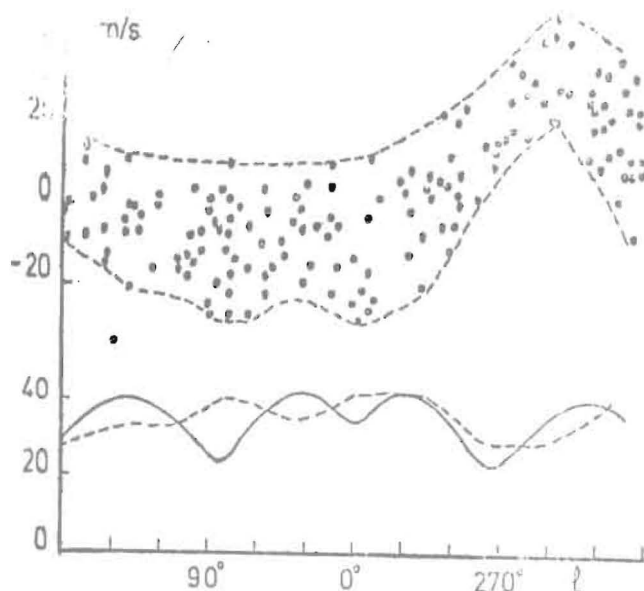


Fig. 6. The same as in Fig. 5 for stars in the distance interval 0 - 1 kpc. Since the distance interval is large we cannot assume that all the stars are at the same distance r . Thus, the theoretical width of the permitted area ΔV (solid line) for the range 0 - 1 kpc is compared to the observed one (dashed line). Two points have been excluded from the tentative permitted area.

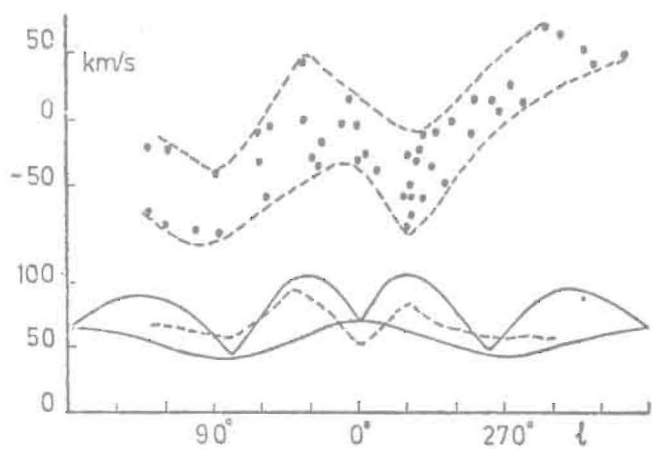


Fig. 7. The same as in Fig. 5 for 50 B-nebulae with distances in the range 0 - 3.5 kpc. Two theoretical curves are shown corresponding to the ranges 0 - 0.1 kpc and 0 - 3.5 kpc (solid lines). A value of 0.1 is taken for the maximum orbital eccentricity.

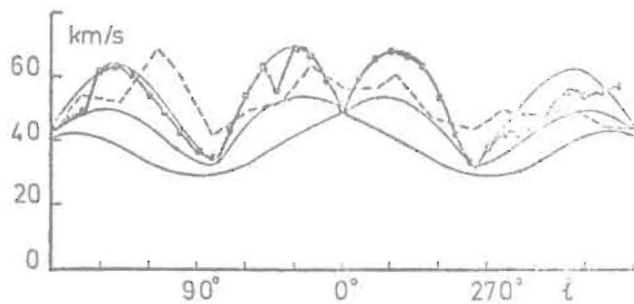


Fig. 8. The width of observed permitted area (dashed line) of supergiants (Humphreys, 1970) with $r < 2$ kpc is compared to the theoretical width (heavy line with dots) obtained by taking the distance of the farthest object within each 20° longitude sector. Those curves in Fig. 3 for $e = 0.07$ are also shown for three values of r , namely, 0.1, 1, and 2 kpc.

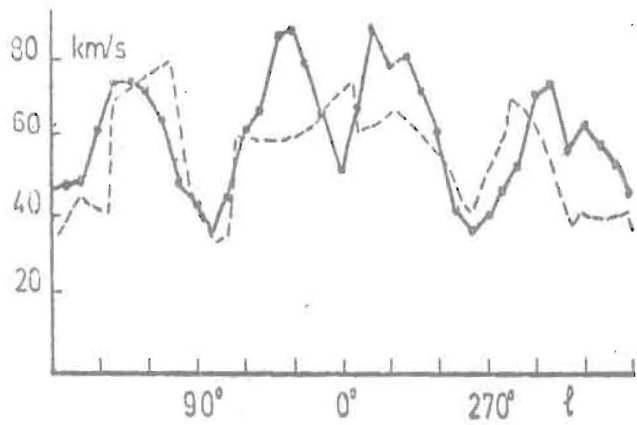


Fig. 9. The same as in Fig. 8 for supergiants with $r < 3$ kpc.

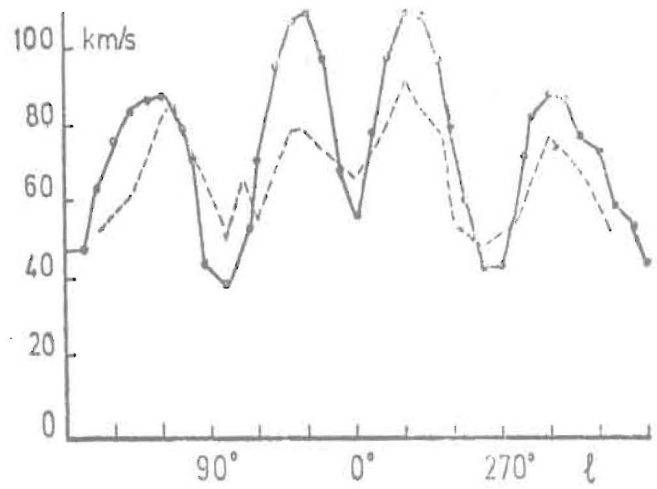


Fig. 10. The same as in Fig. 8 for supergiants with $r < 5$ kpc. Even in the case of a lower assumed eccentricity, say, $e = 0.05$, the observed values at $l \approx 30^\circ$ and $l \approx 330^\circ$ remain smaller than the predicted width of permitted areas at these longitudes.

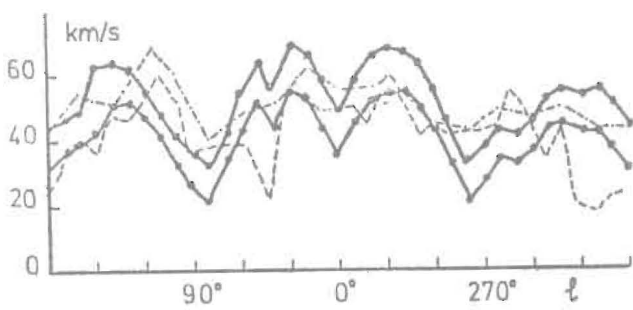


Fig. 11

Fig. 11. Three times the radial-velocity dispersion σ_v (dashed line) for supergiants with $r < 2$ kpc as compared with the results of Fig. 8. The theoretical width of permitted areas for $e = 0.05$ is also shown (lower heavy line with dots).

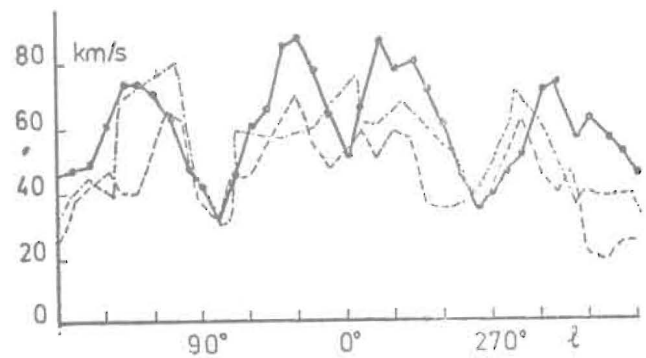


Fig. 12

Fig. 12. The same as in Fig. 11 for supergiants with $r < 3$ kpc. The theoretical curve has been calculated for $e = 0.07$.

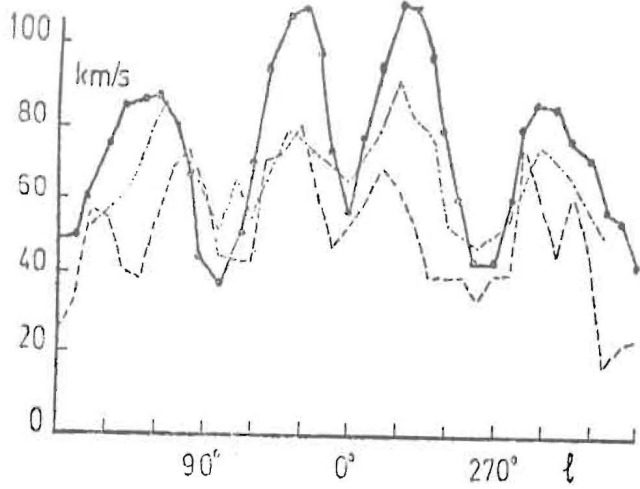


Fig. 13. The same as in Fig. 12 for supergiants with $r < 5$ kpc.

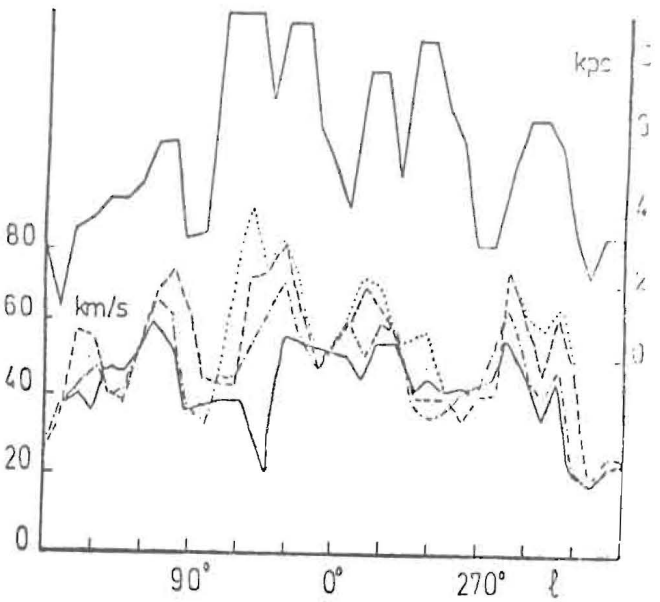


Fig. 14. The uppermost curve represents the distance of the farthest star of the sample plotted against galactic longitude. 20° longitude sectors superimposed 10° have been taken. The lower curves are those of Figs. 11, 12, and 13, corresponding to three times the velocity dispersion σ_v . Dotted line represents the case $r < 10$ kpc, i.e., the whole sample of supergiants.

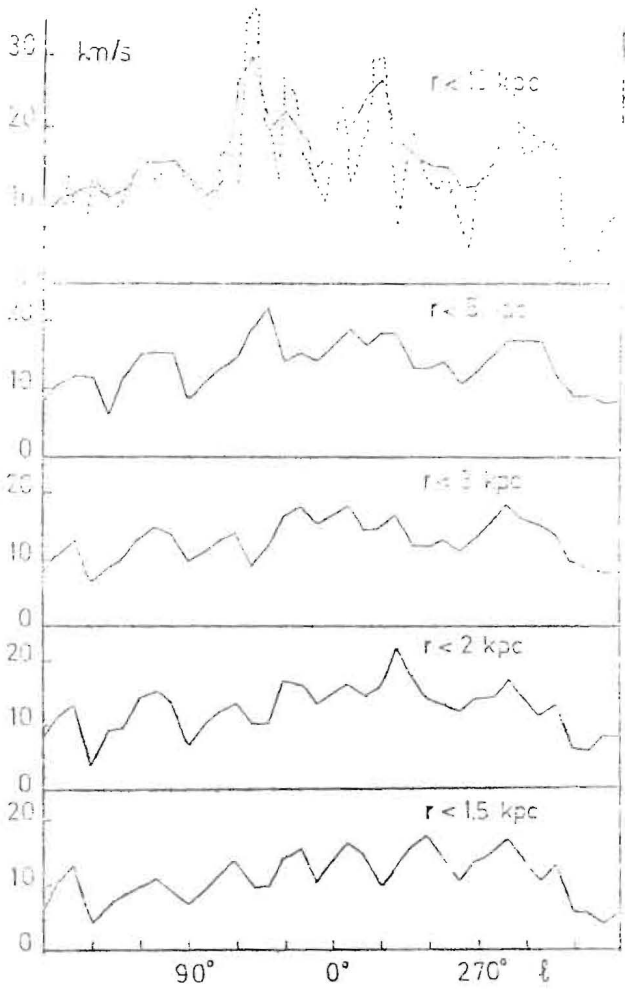


Fig. 15. The dispersion of residuals plotted against galactic longitude for supergiants. The case for $r < 10$ kpc includes all the objects of Humphreys' Catalogue. The other cases correspond to groups of objects with heliocentric distances smaller than a given value. The dotted line represents the dispersion of residuals obtained by taking 10° longitude sectors superimposed 5° . The residuals are calculated by assuming rotational velocities given by the Contopoulos-Strömberg formula.

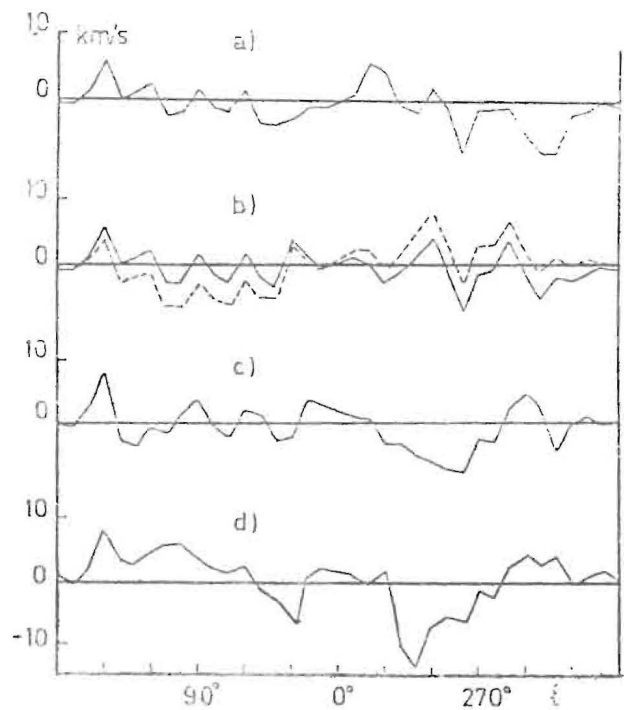


Fig. 16. Average of velocity residuals $\overline{\Delta V_R}$ plotted against galactic longitude. 20° longitude sectors superimposed 10° are taken for calculation. The adopted components of the solar motion are: $U = -9$, $V = 16$ km/s. a) Trend of $\overline{\Delta V_R}$ for the total sample of supergiants. b) $\overline{\Delta V_R}$ for $r < 5$ kpc, dashed line represents the case $U = -9$, $V = 12$ km/s. c) $r < 2$ kpc. d) $r < 1.5$ kpc.

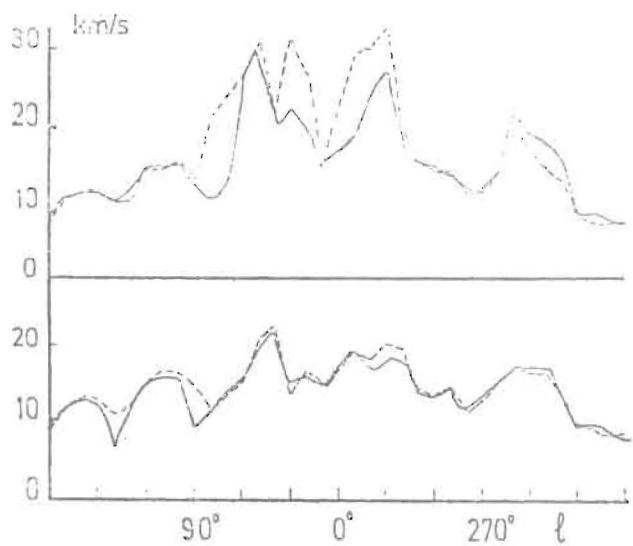


Fig. 17. Dependence of σ_R on the gravitational potential for supergiants. The solid line represents the dispersion of velocity-residuals calculated using the rotational velocities given by the Contopoulos-Strömberg formula. The dashed line represents the dispersion calculated using rotational velocities derived from the potential introduced by Eggen *et al.* (1962). The response of the total sample of supergiants is shown (above) together with the response of a group of objects with $r < 5$ kpc (below).

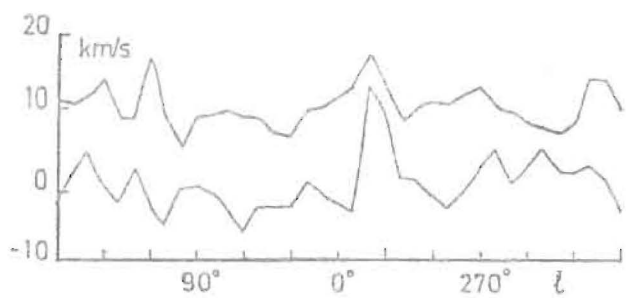


Fig. 18. Dispersion (upper curve) and average (lower curve) of residuals for stars from the catalogues of Fricke *et al.* (1975) and Geyer (1970).

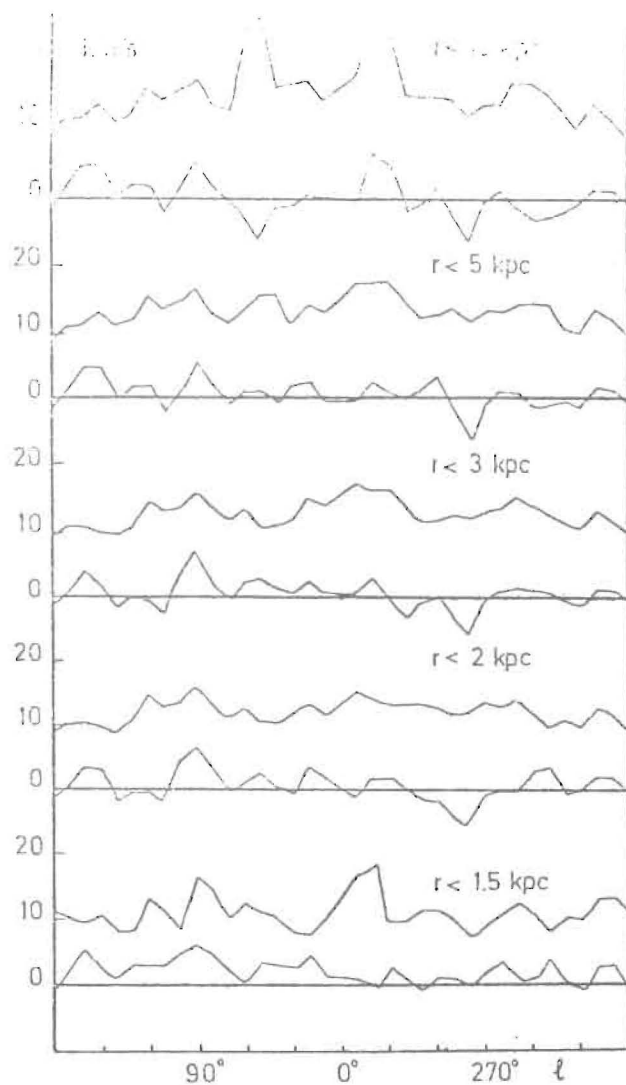


Fig. 19. The same as in Fig. 15 for the total sample of 775 stars contained in the three catalogues mentioned in this paper. The average of residuals are also shown. It is evident that when large-distance objects are included the trend of supergiants becomes dominant:

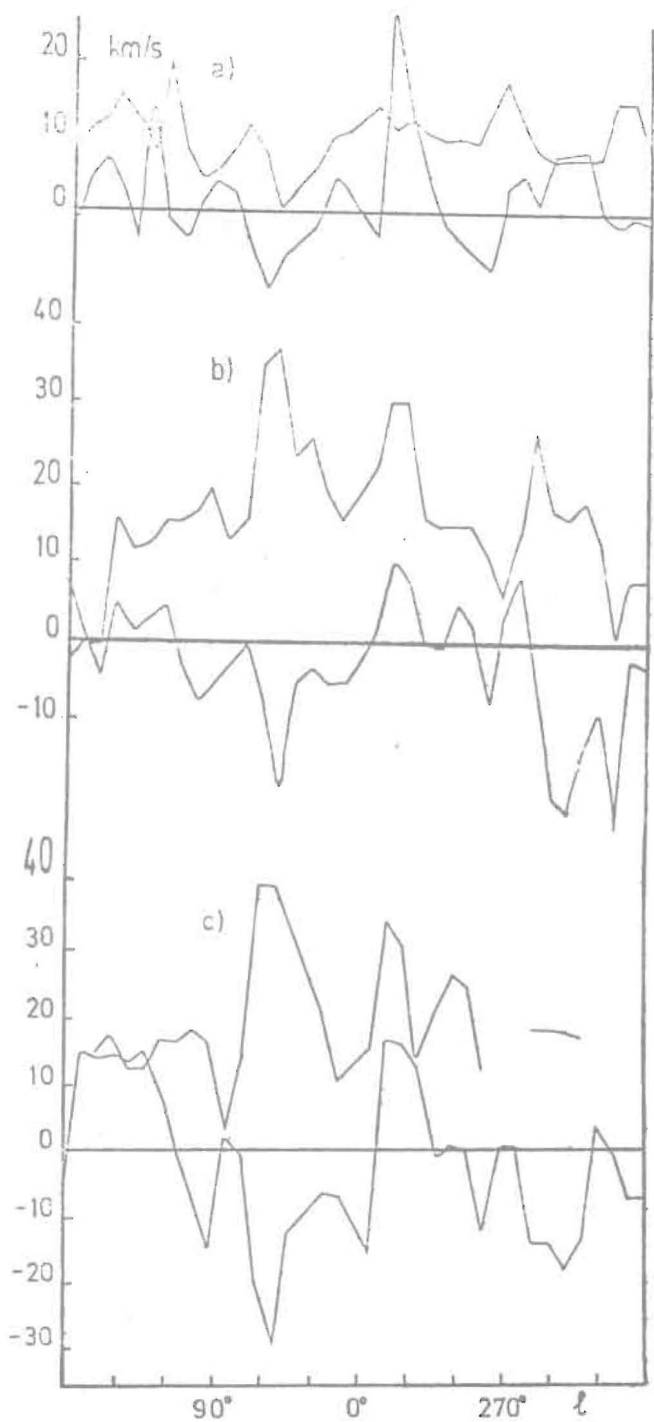


Fig. 20. Dispersion and average of residuals when objects closer to the sun are excluded. a) Stars from the catalogues of Fricke et al. and Geyer with $r > 0.45$ kpc. b) Supergiants with $r \geq 2$ kpc. c) Supergiants with $r \geq 3$ kpc. The discontinuity of the dispersion curve is due to the presence of less than two stars inside the longitude sector. The large-scale trend in $\overline{\Delta V}_R$ observed in Figs 20b and 20c may be explained by assuming a tendency of overestimating distances larger than, say, 2 kpc.

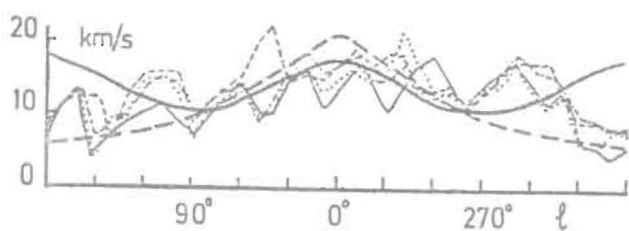


Fig. 21. Dispersions of residuals of supergiants discussed in this paper as compared with the theoretical curves $\Delta V/2$ of Fig. 1b. Heavy solid line corresponds to the theoretical half-width of the permitted area for $r = 0.1$ kpc. Heavy dashed line corresponds to $r = 5$ kpc. The σ_R -curves corresponds to different samples with $r < 5$ kpc discussed in this paper.

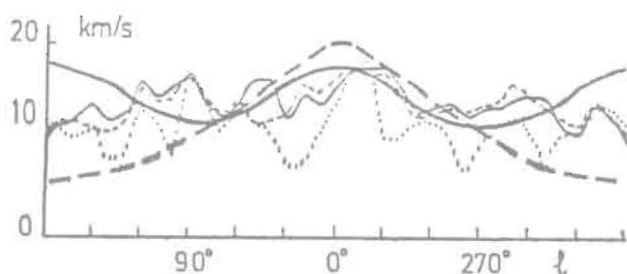


Fig. 22. The same as Fig. 21 for the complete set of 775 stars.

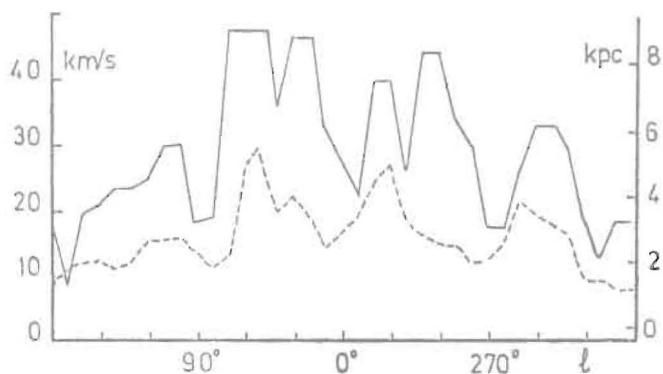


Fig. 23. Residual dispersion of supergiants (dashed line) compared with the distance curve of Fig. 14. The correlation between the peaks of the two curves is evident.

REFERENCES

- Contopoulos, G., Strömberg, B., *Tables of Plane Galactic Orbits*,
New York, NASA Institute for Space Studies, 1965.
- Eggen, O. J., Lynden-Bell, D., Sandage, A. R., *Astrophys. J.*,
Vol. 136, 1962, p. 748.
- Fricke, W., Tsiuimis, A., *Astron. Astrophys.*, Vol. 42, 1975, p.
449.
- Geyer, U., *Astron. Astrophys.*, Vol. 5, 1970, p. 116.
- Greig, W. E., *Astron. Astrophys.*, Vol. 18, 1972, p. 70.
- Humphreys, R. M., *Astron. J.*, Vol. 75, 1970, p. 602.
- Peralta, J. O., *Astron. Astrophys.*, Vol. 54, 1977a, p. 79.
- Peralta, J. O., *Astron. Astrophys.*, (to be published), 1977b.
- Schmidt, M., *Galactic Structure*, Ed. A. Blaauw and M. Schmidt,
Univ. Chicago Press, Chicago, 1965, p. 513.
- Wielen, R., *Pub. Astr. Soc. Pacific.*, Vol. 86, 1974, p. 341.